Alloys and Intermetallics

MS.6.164
In-situ TEM straining of tetragonal martensite in a Ni-Mn-Ga alloy

N. Zárubová[1], Y. Ge[2], O. Heczko[1], S.-P. Hannula[2]

[1]Institute of Physics, ASCR, Department of Functional Materials, Prague 8, Czech Republic
[2]Aalto University, School of Chemical Technology, Departement of Materials Science and Engineering, Aalto, Finland

zarubova@fzu.cz
Keywords: *in-situ* TEM straining, martensitic transformation, Ni-Mn-Ga shape memory alloy

Ni-Mn-Ga is a ferromagnetic shape memory alloy (FSMA) with many potential applications for sensors and actuators. This is based on the fact that large strains can be achieved by application of mechanical, magnetic or combined magneto-mechanical forces [1,2]. The magnetic-field-induced-strain (magnetoplasticity) in Ni-Mn-Ga is caused by the reorientation of martensite variants. The reorientation mechanism in Ni-Mn-Ga has been well explained from the phenomenological point of view [3-5], but there is a discussion about the microscopic mechanism, and only few TEM observations of the reorientation process have been published so far [6-8]. In the present study, the *in-situ* TEM straining tests were performed to follow in detail the reorientation of martensite variants of non-modulated tetragonal martensite (NM), with the aim to explain the mechanism of the twin boundary motion [9].

Foils of $Ni_{52.4}Mn_{27.3}Ga_{20.3}$ alloy (1.67 x 5.5 x 0.1 mm^3) were prepared from a single crystal with NM martensite structure. The central area of the foils was thinned until a hole appeared. The samples were strained in tension at room temperature in a JEM 1200EX microscope equipped with a double-tilt straining stage. The stress-induced processes were video-recorded, and then the structure was examined under stress using two-beam bright and dark field conditions. Some deformed foils were further cut to a 3 mm length and analyzed in a high-resolution Tecnai F20 200kV FEG microscope.

Figure 1a shows the crystallographic orientation of the three tetragonal martensite variants in the foil. M2 is the most favorably oriented variant relative to the external load and M3 is the least preferable one. Figure 1b illustrates two levels of twin hierarchy in the self-accommodated thermally induced martensite. Large domains, separated by incoherent boundaries, consist of internal twins, which form a lamellar structure. The internal twins, about a dozen of nanometers in size, are (101) compound twins, in agreement with the theory of tetragonal martensite. The interfaces between the internal twins (twin planes) are planar and coherent.

After applying the external load, detwinning process starts by movement of twinning dislocations along the internal twin boundaries. The variants oriented more favorably to the applied stress grow at the expense of the less favorable ones. The dislocation speed is very high at the beginning, and a large number of dislocations move simultaneously. As the process successively slows down, movement of individual twinning dislocations can be monitored due to the bow-like contrast, provided that the internal twins are inclined to the foil surface (Figure 1c). The twinning dislocations are starting and ending at the incoherent inter-domain boundaries. The nucleation process is shown in Figure 2a where the dislocations are generated at the intersection of the M3 plate with the domain boundary.

For the variant combination M2+M3 shown in Figures 2a,b the twin planes are ($)_{M2}$ planes. The direction of the Burgers vector of the twinning dislocations, b, is $[101]_{M2}$ as determined from the invisibility criterion, $g \cdot b = 0$ [8]. The pronounced changing contrast on the transforming plates (see Figures 2a,b) is the result of variations in the lattice displacement and twin plate thickness, both due to movement of twinning dislocations on successive twin planes (see the scheme in Figure 2c). The magnitude of the Burgers vector of the twinning dislocations can be determined from the variations of α-fringe contrast on the reorienting twin plates [6]. The changes in the contrast correspond to the phase differences $\alpha = 2\pi(g.b)$, $2\pi(g.2b)$, etc. produced by an array of twinning dislocations with the Burgers vector close to 1/12[101] gliding in the successive ( ) planes.

Our TEM observations agree well with the results of Ref. [6]. For operative reflection g = 022, a train of twining dislocations with the Burgers vector 1/12 [101] will yield a six-fold contrast, $\alpha = \pi/3$, $2\pi/3$, π, $4\pi/3$, $5\pi/3$, 2π. An example is shown in Figure 2b (see also [8]). Six levels of contrast are clearly visible on the transforming M3 plate in the image center. Segment 6 is without contrast, in agreement with $\alpha = 2\pi$ 6/12[101] [022] = 2π. The broad segments of equal contrast shown in Figure 2b often indicate an irregular distribution of the twinning dislocations (Figure 2c, case I), while their arrangement is very regular at the ends of the transforming plates (see double arrows in Figure 2b, and Figure 2c, case II). It is demonstrated in Figures 3a-d, where changes of the contrast with the operative reflection are illustrated. Figure 3d is a dark-field image in reflection 0012_{M2}. The α-contrast disappears in this reflection ($g \cdot b = 1$, $\alpha = 2\pi$) and individual twinning dislocations are visible as fine lines, without disturbance of the α-fringes. The distances between dislocations are about 30nm.

1. K. Ullakko, J.K. Huang, C. Kanter, R.C. O'Handley and V.V. Kokorin, Appl Phys Lett 69 (1996), p. 1966.
2. A. Sozinov, N. Lanska, A. Soroka and W. Zou, Appl Phys Lett 102 (2013), p. 021902.
3. P. Müllner and A.H.King, Acta Mater 58 (2010), p. 5242.
4. O. Heczko, L. Straka, I. Aaltio and S.-P. Hannula, Mater Sci Eng A 481-482 (2008), p. 283.

5. O. Heczko, N. Scheerbaum, O. Gutfleisch, “Magnetic shape memory phenomena”, in Nanoscale magnetic
materials and applications, Springer Science+Business Media (2009), p.399.
6. R.C. Pond, B. Muntifering and P. Müllner, Acta Mater 60 (2012), p. 3976.
7. Y. Ge, N. Zárubová, Z. Dlabáček, I. Aaltio, O. Söderberg and S.-P. Hannulal, Proc. ESOMAT 2009;04007 DOI:
10.1051/esomat/200904007.
8. N. Zárubová, Y. Ge, J. Gemperlová, A. Gemperle and S.-P. Hannula, Func Mater Lett 5 (2012), p. 1250006.
9. N. Zárubová, Y. Ge, O. Heczko and S.-P. Hannula, Acta Mater, submitted.
10. We kindly acknowledge the financial support of the Academy of Finland, Grant Agency of CR (contracts P107/11/0391, P107/12/0800) and Grant Agency of ASCR (contract IAA100100920). Operation of the JEM 1200EX microscope was supported by the grant MEYS of CR LM201126.

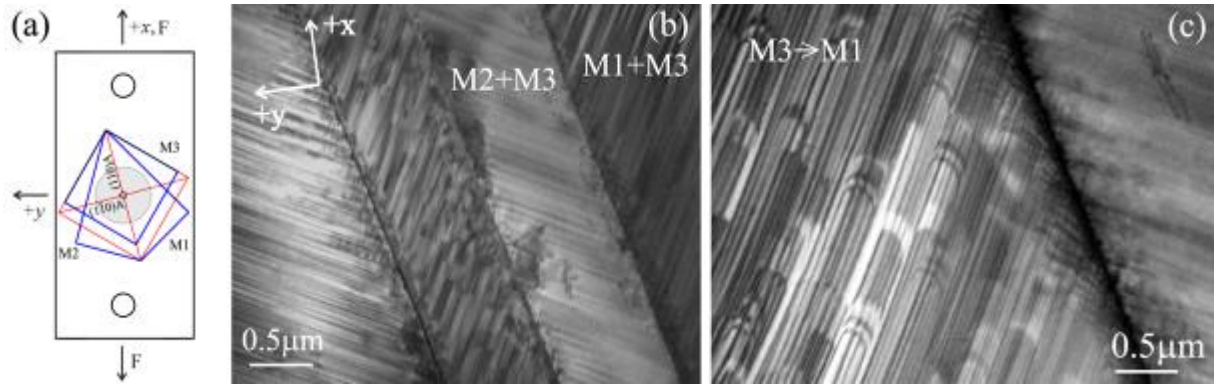

Figure 1. (a) Orientation of the parent austenite (red) and the martensite variants M1, M2, M3 (blue) in the foil. F – external load; *x, y* – tilt axes. (b) Structure of the thermally induced martensite. (c) A video frame recording the detwinning process M3→M1. The twinning dislocations are visualized by the bow-like contrast.

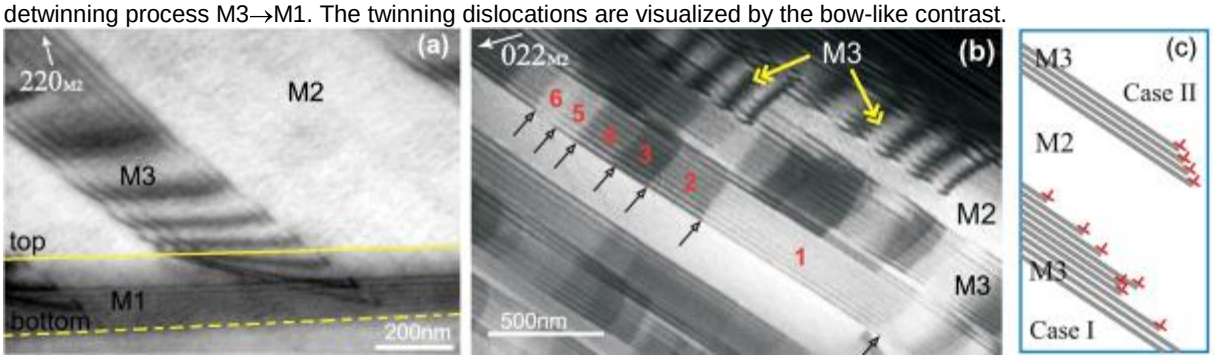

Figure 2. (a) Nucleation of twinning dislocations at the intersection of the M3 plate with the boundary between two domains. (b) Partly detwinned domain M2+M3. Plates of M3 variant reorient into M2 variant. Positions of the twinning dislocations and six levels of the contrast are marked by the black arrows. (c) A scheme of twinning dislocations gliding in parallel twin planes. The twin planes are perpendicular to the plane of the scheme.

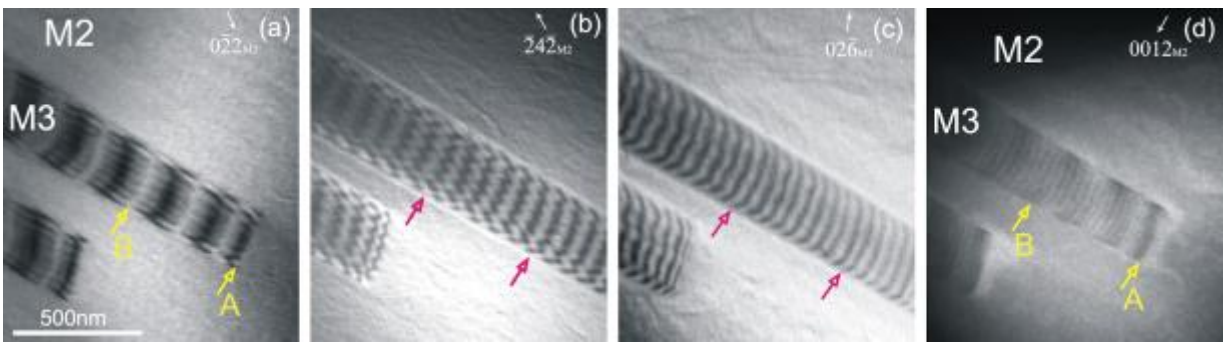

Figure 3. Contrast on reorienting M3 plates in various reflections. (a) **g**·**b** = 1/6; six-level contrast. (b) **g**·**b** = -1/3; three-level contrast. (c) **g**·**b** = -1/2; two-level contrast. (d) **g**·**b** = 1; α-contrast vanished; only dislocations are visible.